# Supplementary Information (SI)

## The single-crystal to single-crystal transformation in pentagonal bipyramidal Fe(II) complex with $N_3S_2$ chelating ligand: switching on single-ion magnet properties via axial ligand substitution

Leokadiya V. Zorina,*[a] Sergey V. Simonov,[a] Valentina D. Sasnovskaya,[b] Maxim A. Blagov,[b] Denis V. Korchagin,[b] Mikhail V. Zhidkov,[b] Alexei I. Dmitriev,[b] Evgenii V. Khramov [c] and Eduard B. Yagubskii [b]

*[a]Osipyan Institute of Solid State Physics, Russian Academy of Sciences, Chernogolovka, Moscow district, 142432, Russia. E-mail: zorina@issp.ac.ru*
*[b]Federal Research Center of Problems of Chemical Physics and Medicinal Chemistry, Russian Academy of Sciences, Chernogolovka, Moscow district, 142432, Russia. E-mail: yagubski@gmail.com*
*[c]National Research Center Kurchatov Institute, Moscow, 123182, Russia*

**Contents:**

**Table S1**. Selected bond lengths (Å) and angles (°) in PBP Fe(II) complexes **1** and **2**.

| Bond | **1** | **2** |
|---|---|---|
| Fe(1)-S(1) | 2.5764(7) | 2.604(10) |
| Fe(1)-N(2) | 2.3086(17) | 2.30(2) |
| Fe(1)-N(3) | 2.180(2) | 2.26(3) |
| Fe(1)-O(1) | 2.1446(18) | - |
| Fe(1)-Cl(1) | - | 2.531(8) |
| **Angle** | **1** | **2** |
| S(1)-Fe(1)-S(1)* | 73.04(3) | 73.3(4) |
| S(1)-Fe(1)-N(2) | 73.04(4) | 73.0(6) |
| S(1)-Fe(1)-N(3) | 143.481(14) | 143.3(2) |
| S(1)-Fe(1)-N(2)* | 145.35(5) | 145.7(7) |
| N(2)-Fe(1)-N(3) | 70.71(4) | 70.6(6) |
| N(2)-Fe(1)-N(2)* | 141.43(9) | 141.1(13) |
| S(1)-Fe(1)-O(1) | 94.29(5) | |
| S(1)-Fe(1)-O(1)* | 90.43(5) | |
| N(2)-Fe(1)-O(1) | 85.26(6) | |
| N(2)-Fe(1)-O(1)* | 92.80(6) | |
| N(3)-Fe(1)-O(1) | 87.07(5) | |
| O(1)-Fe(1)-O(1)* | 174.13(9) | |
| Fe(1)-O(1)-C(15) | 130.60(17) | |
| S(1)-Fe(1)-Cl(1) | | 94.4(3) |
| S(1)-Fe(1)-Cl(1)* | | 88.2(3) |
| N(2)-Fe(1)-Cl(1) | | 87.5(6) |
| N(2)-Fe(1)-Cl(1)* | | 91.4(6) |
| N(3)-Fe(1)-Cl(1) | | 88.4(2) |
| Cl(1)-Fe(1)-Cl(1)* | | 176.8(5) |

(*) Symmetry code: (1.5-x, y, 1-z).

**Table S2.** SHAPE* analysis of the Fe(II) complexes with 7-vertex polyhedra in **1** and **2**.

| Complex | HP-7 | HPY-7 | **PBPY-7** | COC-7 | CTPR-7 | JPBPY-7 | JETPY-7 |
|---|---|---|---|---|---|---|---|
| **1** | 33.997 | 24.661 | **0.770** | 7.492 | 5.838 | 2.571 | 24.340 |
| **2** | 35.191 | 26.476 | **0.493** | 7.420 | 5.730 | 4.900 | 24.411 |

HP-7 - Heptagon ($D_{7h}$); HPY-7 - Hexagonal pyramid ($C_{6v}$); **PBPY-7 - Pentagonal bipyramid ($D_{5h}$)**; COC-7 - Capped octahedron ($C_{3v}$); CTPR-7 - Capped trigonal prism ($C_{2v}$); JPBPY-7 - Johnson pentagonal bipyramid J13 ($D_{5h}$); JETPY-7 - Johnson elongated triangular pyramid J7 ($C_{3v}$)

* [M. Llunell, D. Casanova, J. Cirera, P. Alemany, S. Alvarez, 'SHAPE: Program for the Stereochemical Analysis of Molecular Fragments by Means of Continuous Shape Measures and Associated Tools', Version 2.1, 2013, Barcelona]

**Table S3.** H-bond geometry in structure **1**.

| Donor--H..Acceptor | [Symmetry of A] | D-H, Å | H...A, Å | D...A, Å | D-H...A, º |
|---|---|---|---|---|---|
| N1 --H1n ..Cl1 | [1.5-x,0.5-y,0.5-z] | 0.87(3) | 2.41(2) | 3.206(2) | 153(1) |
| N4 --H4n ..Cl1 | [1.5-x,0.5-y,0.5-z] | 0.88(3) | 2.29(2) | 3.145(2) | 165(1) |
| C3 --H3 ..S1 | [x,y,z] | 0.95 | 2.49 | 3.178(2) | 129.5 |
| C4 --H4 ..O2 | [x-0.5,1-y,z] | 0.95 | 2.47 | 3.357(4) | 154.6 |
| C10 --H10a ..Cl1 | [1.5-x,0.5-y,0.5-z] | 0.98 | 2.97 | 3.783(3) | 140.8 |
| C14 --H14 ..O2 | [x-0.5,-y,z] | 0.95 | 2.27 | 3.153(5) | 153.5 |
| O1 --H1s ..Cl1 | [x,y,z] | 0.83(3) | 2.21(2) | 3.028(2) | 168(1) |
| O2 --H2s ..Cl1 | [x,y,z] | 0.85(7) | 2.38(7) | 3.202(4) | 162(3) |

**Table S4.** H-bond geometry in structure **2**.

| Donor--H..Acceptor | [Symmetry of A] | D-H, Å | H...A, Å | D...A, Å | D-H...A, º |
|---|---|---|---|---|---|
| N1 --H1n ..Cl1 | [1.5-x,0.5-y,0.5-z] | 0.88 | 2.45 | 3.25(2) | 151.1 |
| N4 --H4n ..Cl1 | [1.5-x,0.5-y,0.5-z] | 0.88 | 2.39 | 3.24(3) | 162.7 |
| C3 --H3 ..S1 | [x,y,z] | 0.95 | 2.60 | 3.26(4) | 127.4 |
| C6 --H6 ..Cl1 | [x-0.5,y+0.5,z-0.5] | 0.95 | 2.85 | 3.71(3) | 152.4 |
| C10 --H10c ..S1 | [1.5-x,0.5-y,0.5-z] | 0.98 | 2.95 | 3.87(4) | 156.5 |

**Table S5.** Mössbauer parameters for spectra of powder $[Fe^{II}(H_2L)(MeOH)_2]Cl_2\cdot MeOH$ (**1**) and $[Fe^{II}(L)Cl_2]$ (**2**) at 80 and 296 K. $\Delta E_Q$ – quadrupole splitting; δ – isomer shift; Γ – line width; S – contribution of subspectrum in percent.

| Sample | T, K | $\Delta E_Q$, mm/s | δ, mm/s | Γ, mm/s | S, % |
|---|---|---|---|---|---|
| **1**, *(a)* | 80 | 3.59(1) | 1.20(1) | 0.27(2) | 100 |
| **1**, (*b*) | 296 | 3.02(4) | 1.08(2) | 0.31(6) | 30 |
|  |  | 1.37(1) | 1.06(1) | 0.27(2) | 70 |
| **1**, (*c*) | 296 | 1.35(1) | 1.07(1) | 0.26(1) | 100 |
| **2** | 296 | 1.33(1) | 1.07(1) | 0.30(1) | 100 |
|  | 80 | 1.74(1) | 1.20(1) | 0.37(1) |  |

**Table S6.** Calculated spin-free and spin orbit (SO) energies (cm$^{-1}$) of the lowest ten term and states for **1** and **2** using SA-CASSCF/SA-NEVPT2 approach.

| **Complex** | **1** | | **2** | |
|---|---|---|---|---|
| **№ of state** | **Spin free states** | **SO states** | **Spin free states** | **SO states** |
| 1 | 0.0 | 0.00 | 0.0 | 0.00 |
| 2 | 1239.9 | 2.27 | 80.6 | 0.10 |
| 3 | 5648.4 | 12.14 | 3067.2 | 70.22 |
| 4 | 5855.7 | 25.78 | 3666.5 | 70.70 |
| 5 | 9534.2 | 27.61 | 7601.9 | 118.91 |
| 6 | 13675.9 | 902.83 | 13613.3 | 247.52 |
| 7 | 18679.9 | 909.75 | 17945.3 | 291.58 |
| 8 | 18884.7 | 937.08 | 18142.0 | 332.93 |
| 9 | 19486.5 | 972.96 | 18715.5 | 424.62 |
| 10 | 19754.8 | 976.11 | 18818.5 | 425.07 |

**Table S7.** Experimental X-ray diffraction resolution statistics for **2**.

| resolution(Å) | # kept | # theor. | # uniq. | % compl. | av.redundancy | mean $F^2$ | mean $F^2/\sigma(F^2)$ | $R_{int}$ | $\sigma$ | $CC^{1/2}$ | CC* |
|---|---|---|---|---|---|---|---|---|---|---|---|
| 10.80-1.80 | 1180 | 289 | 287 | 99.3 | 4.1 | 19.12 | 10.95 | 0.057 | 0.043 | 0.999 | 1.000 |
| 1.80-1.42 | 1229 | 289 | 289 | 100.0 | 4.3 | 3.97 | 2.66 | 0.151 | 0.130 | 0.995 | 0.999 |
| 1.42-1.24 | 1205 | 289 | 289 | 100.0 | 4.2 | 1.11 | 0.55 | 0.357 | 0.278 | 0.953 | 0.988 |
| 1.24-1.12 | 1191 | 289 | 289 | 100.0 | 4.1 | 2.30 | 1.99 | 0.380 | 0.290 | 0.925 | 0.980 |
| 1.12-1.04 | 1214 | 289 | 289 | 100.0 | 4.2 | 2.64 | 2.66 | 0.393 | 0.320 | 0.879 | 0.967 |
| 1.04-0.98 | 1223 | 289 | 289 | 100.0 | 4.2 | 3.31 | 3.07 | 0.341 | 0.310 | 0.826 | 0.951 |
| 0.98-0.93 | 1183 | 289 | 289 | 100.0 | 4.1 | 2.54 | 2.49 | 0.408 | 0.399 | 0.622 | 0.876 |
| 0.93-0.89 | 1203 | 289 | 289 | 100.0 | 4.2 | 1.04 | 1.09 | 0.661 | 0.663 | 0.624 | 0.877 |
| 0.89-0.85 | 1186 | 289 | 289 | 100.0 | 4.1 | -0.70 | -0.86 | 0.716 | 0.664 | 0.563 | 0.849 |
| 0.85-0.82 | 1009 | 292 | 280 | 95.9 | 3.6 | -2.50 | -2.37 | 0.497 | 0.424 | 0.475 | 0.803 |
| 10.80-0.82 | 11823 | 2893 | 2879 | 99.5 | 4.1 | 3.36 | 2.29 | 0.239 | 0.198 | 0.997 | 0.999 |

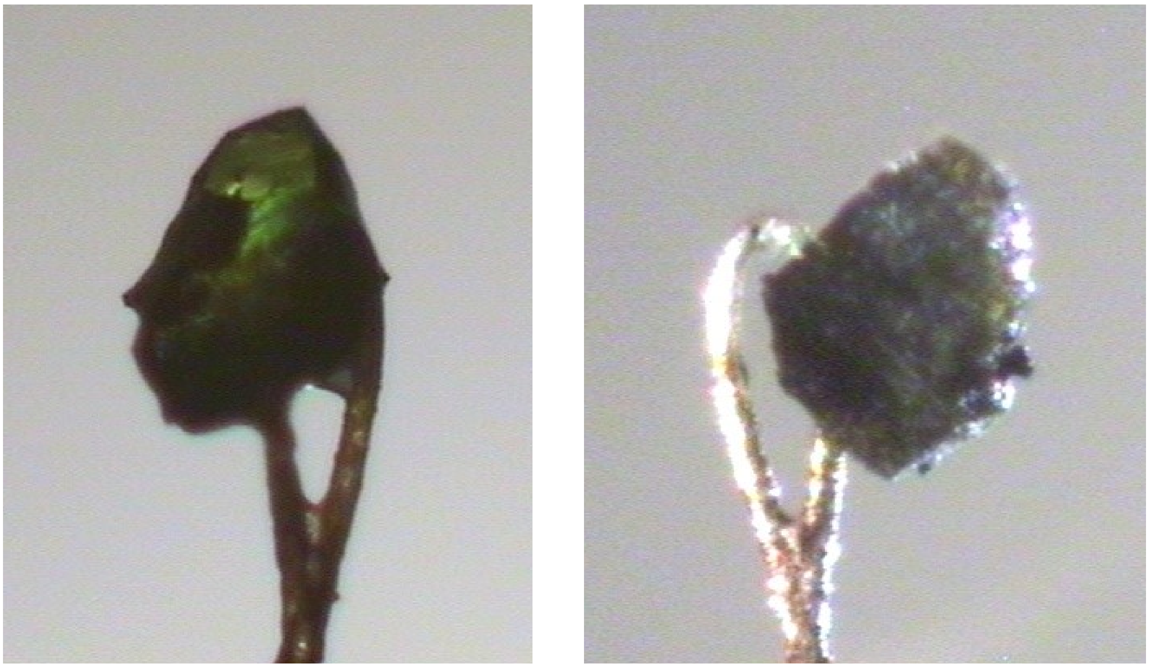

(a) (b)

**Figure S1.** Photographs of the octahedron-shaped crystal of complex **1** taken from the mother liquor and placed into a cold (200 K) nitrogen stream of diffractometer (a) and the same crystal after drying at room temperature and conversion to complex **2** (b). The transformed crystal looses transparency and cracks into lamellas (see Fig. S2a).

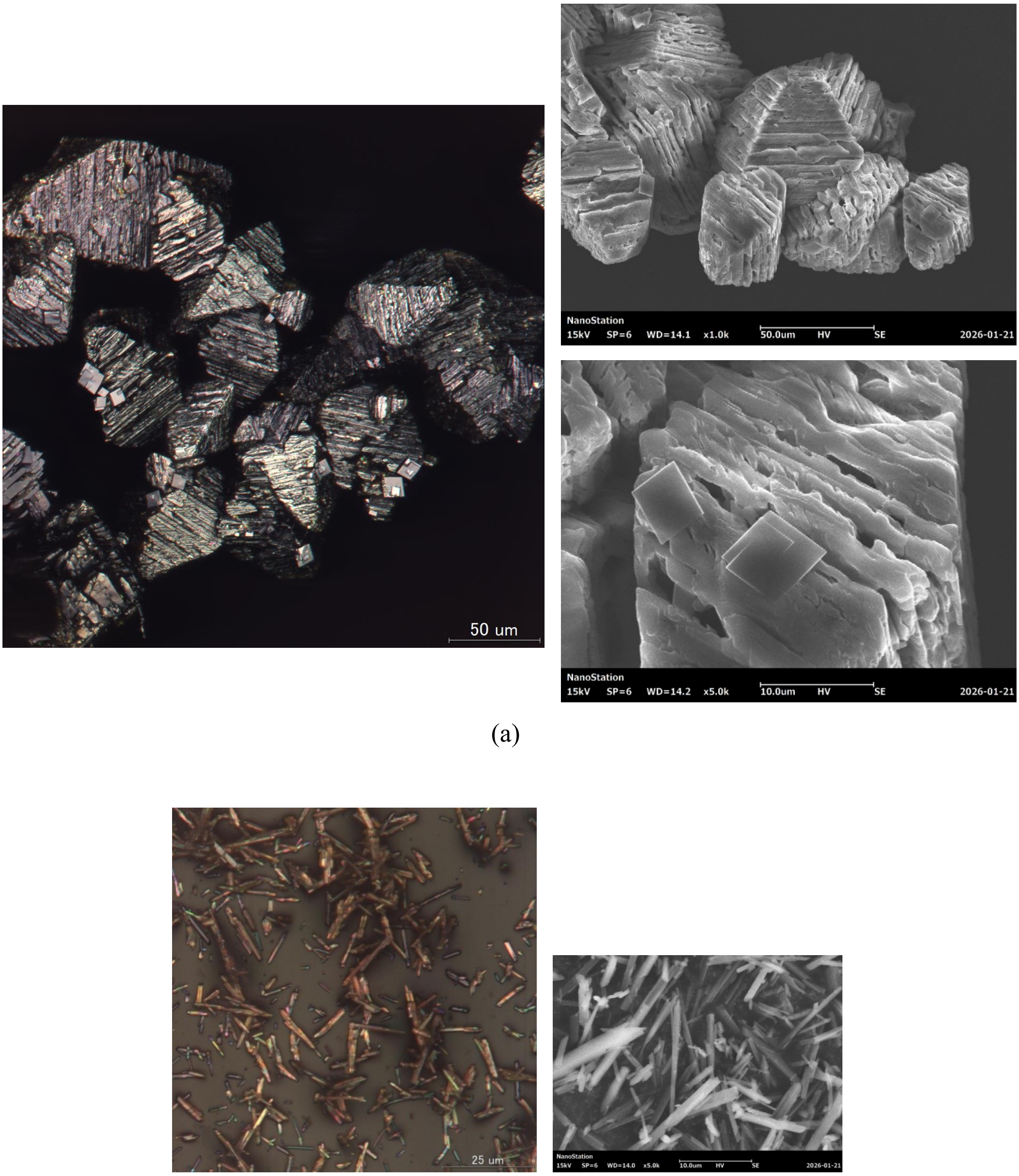

(a)

(b)

**Figure S2.** OM (left) and SEM (right) images of dried octahedron-shaped crystals of complex **1** after SC-SC transformation into complex **2** (a) and small needle-shaped crystals of complex **2** in the sample synthesized as a fine-crystalline precipitate (b).

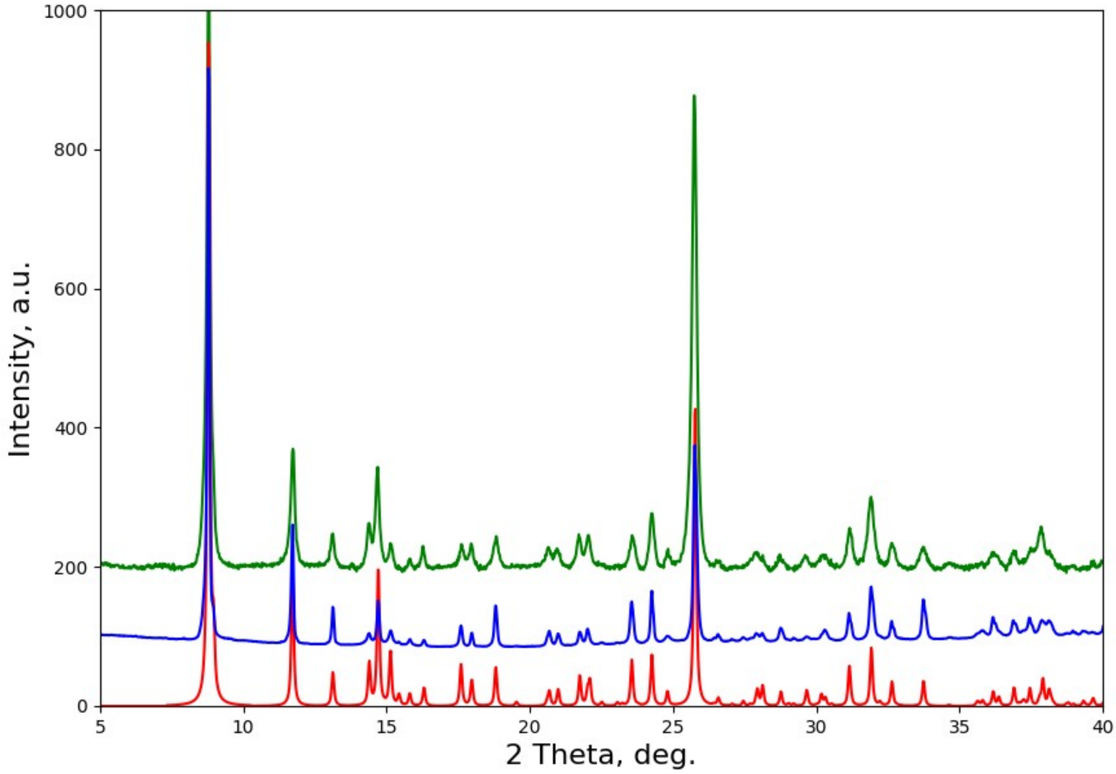

**Figure S3**. Powder XRD spectra of **2**: green – bulk sample obtained by air drying of **1**, blue – sample **2** synthesized as a fine-crystalline precipitate (see Experimental), red – calculated from SXRD data. Physical measurements were carried out on the purest sample **2** (blue spectrum).

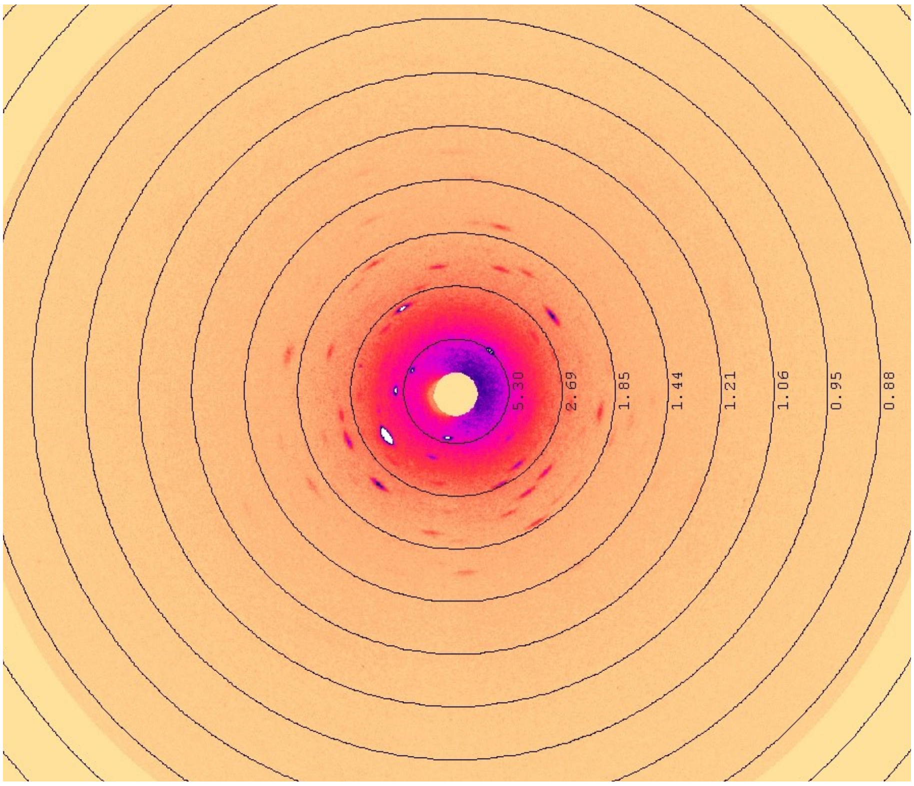

**Figure S4.** Example of diffraction pattern from crystal **2** with highly diffuse reflections at low θ angles.

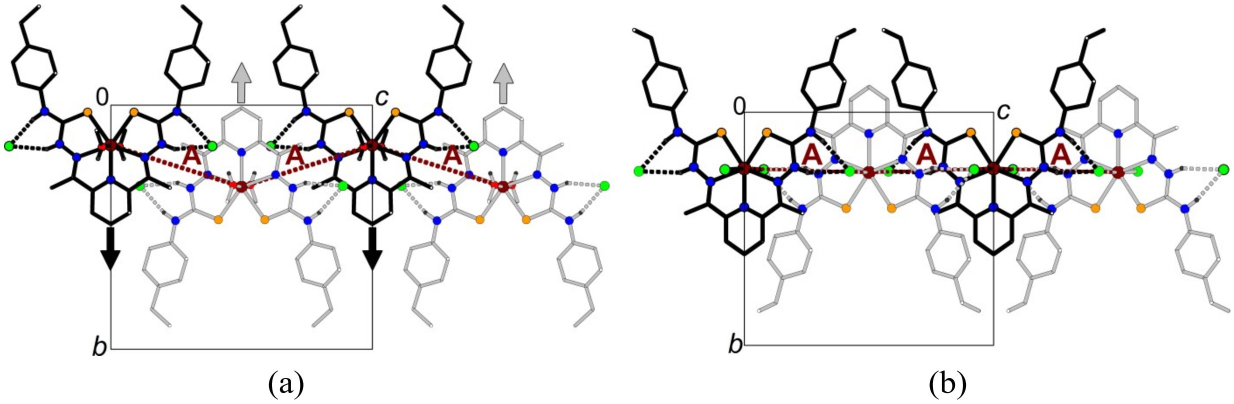

**Figure S5.** Chain of the interactions A in structure **1** (a) and **2** (b). Arrows mark movement of the robust H-bonded Cl…Fe($H_2L$)…Cl fragments (black and grey) after removal of the MeOH ligands.

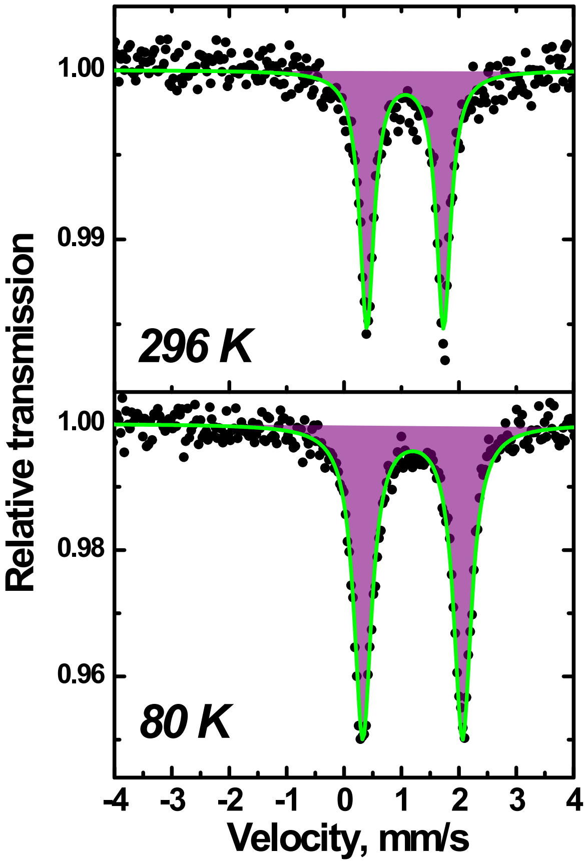

**Figure S6.** Mössbauer spectra of powder $[Fe^{II}(H_2L)Cl_2]$ (**2**) at 80 and 296 K. An area of doublet highlighted in purple corresponds to complex **2**. Green line denotes fit line.

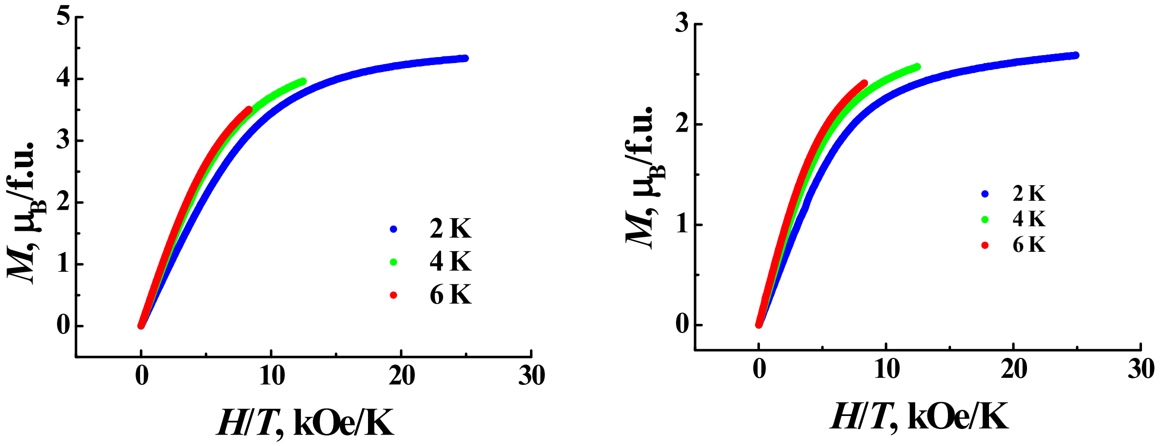

(a) (b)

**Figure S7.** Dependences of magnetization M for **1** (a) and **2** (b) in M(H/T) coordinates, measured at temperatures T = 2 K, 4 K, and 6 K.

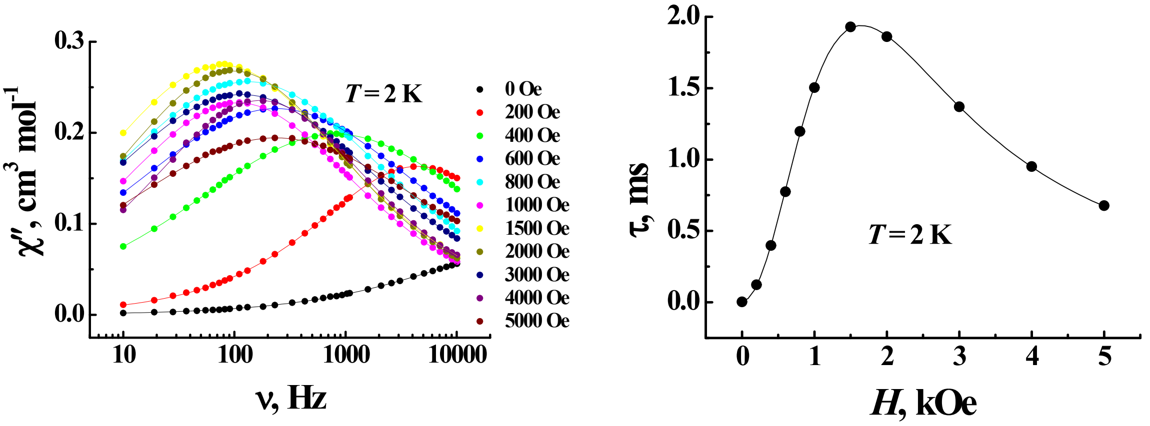

*a*) *b*)

**Figure S8.** a) Frequency dependences of the out-of-phase *ac* magnetic susceptibility for **2** measured in different fields at a temperature of 2 K. Solid lines show the fits by the generalized Debye model. b) Dependence of the relaxation time on the magnitude of the applied *dc* field for for **2** at $T$ = 2 K.

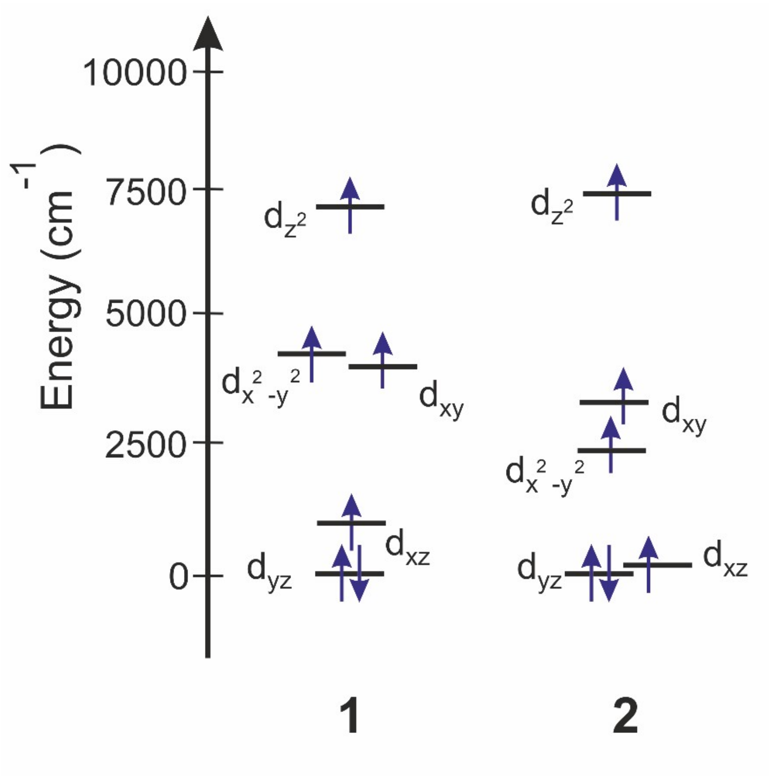

**Figure S9.** d-orbital splitting in **1** and **2**.

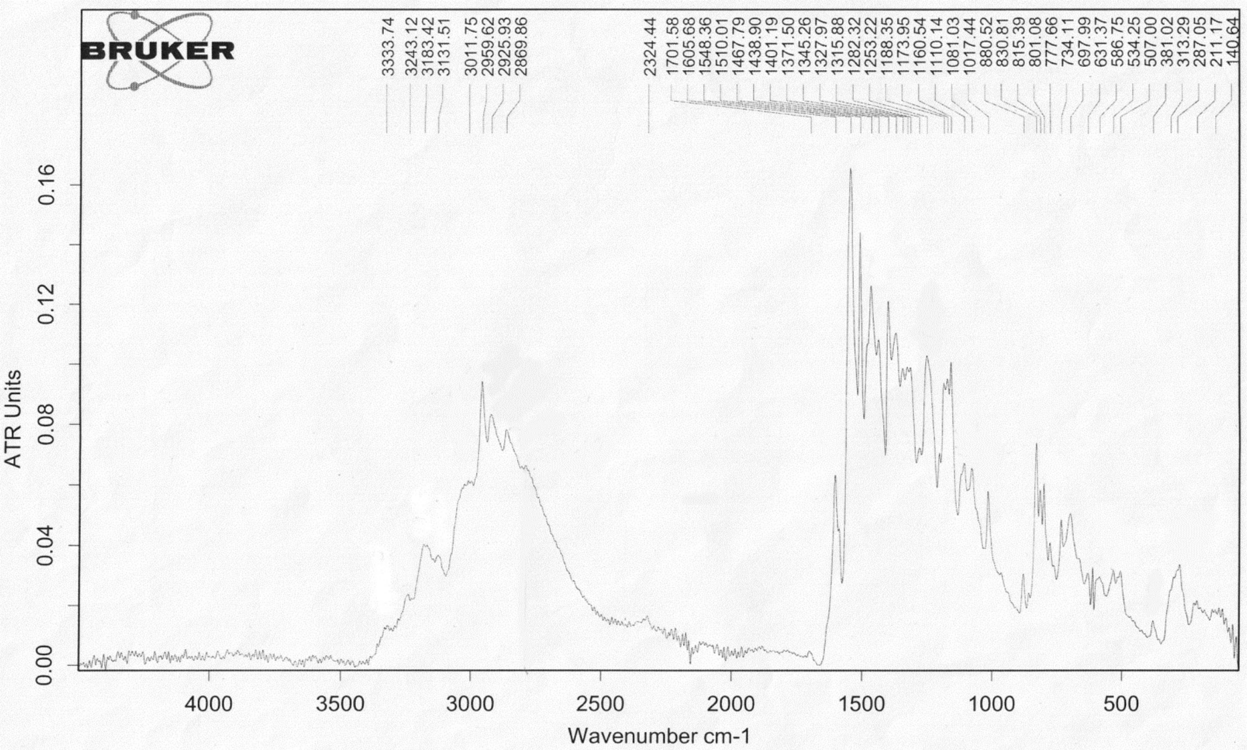

**Figure S10.** Experimental IR absorption spectrum for **1**.

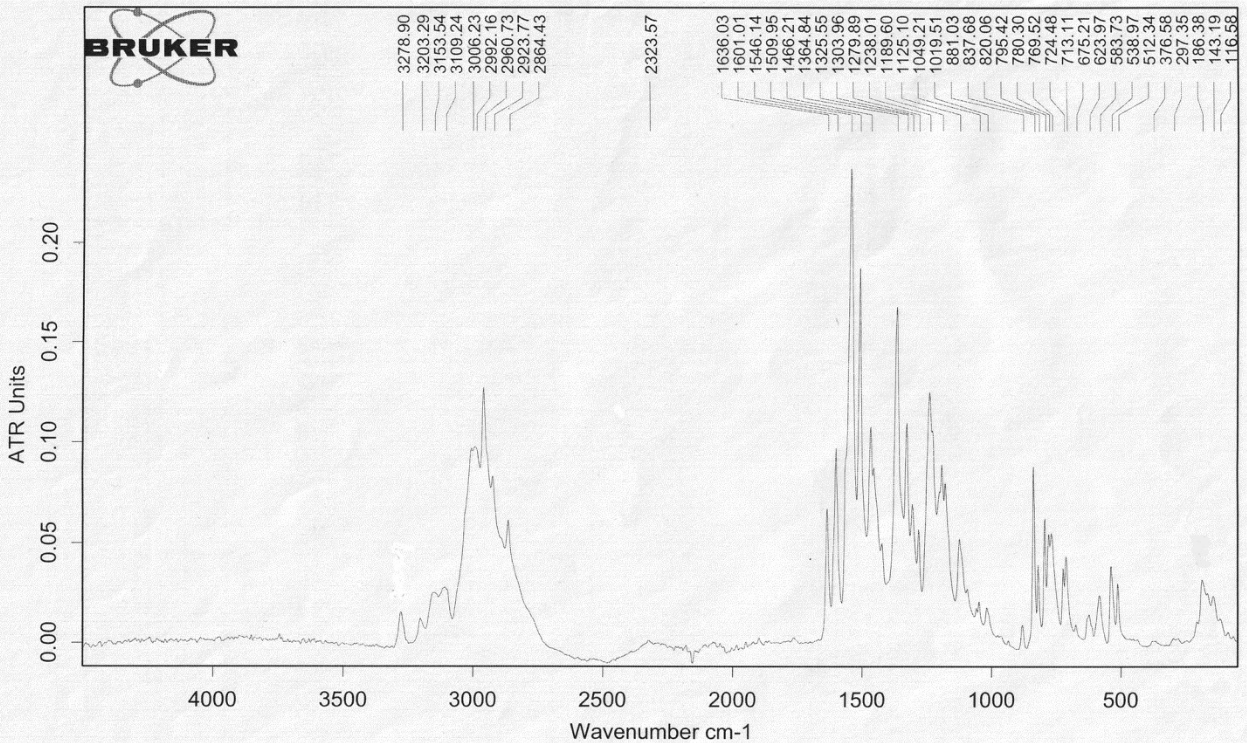

**Figure S11.** Experimental IR absorption spectrum for **2**.

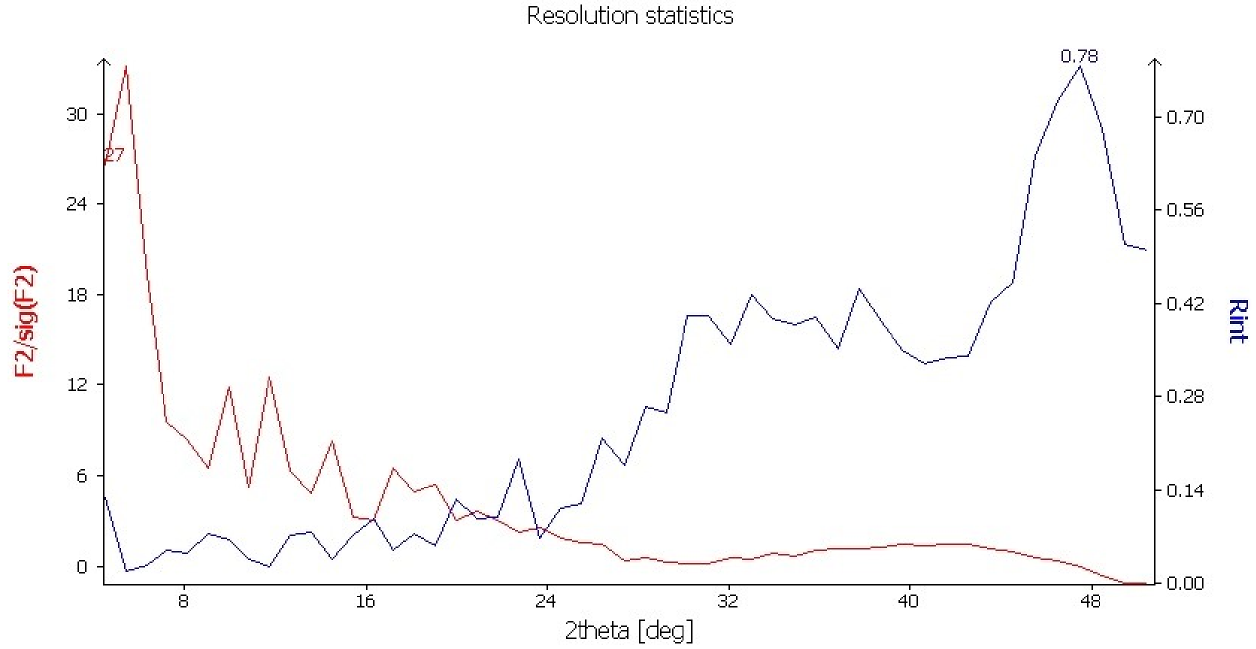

**Figure S12.** $I/\sigma(I)$ and $R_{\text{int}}$ dependencies on 2θ angle for **2**. The experimental diffraction data were cut at $2\theta = 41°$. The observed problems at higher resolution are most likely caused by the cracking of the octahedron-shaped crystals into lamellas upon the SC-SC transformation of **1** to **2** (Fig. S2a) resulting in the diffuse character of all diffraction peaks and the absence of notable intensities at high 2θ angles (Fig. S4, Table S7). All attempts to prevent the crystal cracking by heating it very slowly or placing the crystal in a drop of oil to gradually transform structure **1** into **2** did not lead to the desired result.